

Underwater Acoustic Target Recognition based on Smoothness-inducing Regularization and Spectrogram-based Data Augmentation

Ji Xu^{a,b,*}, Yuan Xie^{a,b,1} and Wenchao Wang^{a,b}

^aKey Laboratory of Speech Acoustics and Content Understanding, Institute of Acoustics, Chinese Academy of Sciences, No.21, Beisihuan West Road, Haidian District, 100190, Beijing, China

^bUniversity of Chinese Academy of Sciences, No.80, Zhongguancun East Road, Haidian District, 100190, Beijing, China

ARTICLE INFO

Keywords:

Underwater acoustic target recognition
Deep learning
Neural network
Regularization
Data augmentation

ABSTRACT

Underwater acoustic target recognition is a challenging task owing to the intricate underwater environments and limited data availability. Insufficient data can hinder the ability of recognition systems to support complex modeling, thus impeding their advancement. To improve the generalization capacity of recognition models, techniques such as data augmentation have been employed to simulate underwater signals and diversify data distribution. However, the complexity of underwater environments can cause the simulated signals to deviate from real scenarios, resulting in biased models that are misguided by non-true data. In this study, we propose two strategies to enhance the generalization ability of models in the case of limited data while avoiding the risk of performance degradation. First, as an alternative to traditional data augmentation, we utilize smoothness-inducing regularization, which only incorporates simulated signals in the regularization term. Additionally, we propose a specialized spectrogram-based data augmentation strategy, namely local masking and replicating (LMR), to capture inter-class relationships. Our experiments and visualization analysis demonstrate the superiority of our proposed strategies.

1. Introduction

Underwater acoustic target recognition is a crucial component of marine acoustics (Brooker and Humphrey, 2016; Xie, Ren and Xu, 2022b), with widespread application in automating maritime traffic monitoring and noise source identification in ocean environmental monitoring systems (Fillinger, de Theije, Zampolli, Sutin, Salloum, Sedunov and Sedunov, 2010; Xie, Ren and Xu, 2022a). The accurate recognition of targets based on radiated noise has high practical value. In recent years, research aimed at building robust underwater acoustic recognition systems has grown significantly due to the increasing demand (Li, Li, Chen and Yu, 2017; Ke, Yuan and Cheng, 2020). Classic paradigm converts signals into non-redundant acoustic features for subsequent recognition. For example, Das et al. (Das, Kumar and Bahl, 2013) employed a cepstrum-based approach for marine vessel classification, Wang and Zeng (Wang and Zeng, 2014) used a bark-wavelet analysis combined with the Hilbert-Huang transform, and Chen et al. (Chen, Han, Ma and Zhang, 2021) used LOFAR (low frequency analysis recording) to reflect the power spectrum distribution and signals changes in time and frequency dimensions. However, Irfan et al. (Irfan, Jiangbin, Ali, Iqbal, Masood and Hamid,

2021) indicated that conventional methods based on low-dimensional acoustic features have limitations on large-scale data with a diversified feature space. They pointed out that high-dimensional representations of acoustic signals could better capture the inherent characteristics of target signals.

With the rapid development of deep learning (LeCun, Bengio and Hinton, 2015) and the accumulation of underwater acoustic databases (Irfan et al., 2021; Santos-Domínguez, Torres-Guijarro, Cardenal-López and Pena-Gimenez, 2016), recognition algorithm based on deep learning continues to grow in popularity. Applying neural networks to learn from high-dimensional spectrograms, which contain rich time-frequency information, has become a prevalent paradigm. For instance, Zhang et al. (Zhang, Da, Zhang and Hu, 2021) used the short-time Fourier transform (STFT) amplitude spectrogram, STFT phase spectrogram, and bi-spectrogram features as inputs for the convolutional neural network (CNN) (Krizhevsky, Sutskever and Hinton, 2012). In addition, spectrograms based on Mel filter banks (Liu, Shen, Luo, Zhao and Guo, 2021; Courmontagne, Ouelha and Chaillan, 2012), Gabor transform (Ren, Xie, Zhang and Xu, 2022), and wavelet transform (Xie et al., 2022a) are also widely applied in CNN-based underwater acoustic recognition. Compared to low-dimensional acoustic features, time-frequency-based spectrograms provide comprehensive information, while neural networks can adaptively capture the deep semantic information and inherent characteristics in spectrograms (Liu et al., 2021; Xie, Xiao, Liu, Liu, Jiang and Qin, 2020; Zhu, Wang, Zhang, Li and Wu, 2021).

Despite advances brought by neural network-based methods, the scarcity of data hinders comprehensive modeling of the complex underwater acoustic environment (Irfan

*Corresponding author

✉ xuji@hcc1.ioa.cn.cn (J. Xu); xieyuan@hcc1.ioa.cn.cn (Y. Xie);

wangenchao@hcc1.ioa.cn.cn (W. Wang)

ORCID(s): 0000-0002-3754-228X (J. Xu); 0000-0003-3803-0929 (Y. Xie)

¹Co-first author.

²The source code of this paper could be obtained from <https://github.com/xy980523/SmoothReg-LMR-DataPrune-underwater-acoustic-recognition>.

arXiv:2306.06945v3 [cs.SD] 30 Apr 2024

et al., 2021; Santos-Domínguez et al., 2016; Gao, Chen, Wang and He, 2020). Limited data cause models to suffer from severe overfitting problems (Xie et al., 2022b), thus seriously hurting the performance and generalization ability of recognition models in real scenarios. To overcome the overfitting problem, researchers often augment training data by simulating underwater signals and generating noisy samples. Some researchers analyze the acoustic characteristics of underwater environments and manually design environment-related noisy samples (e.g., simulate different levels of marine turbulence (Huang, Zhou, Yang, Zhang, Qi and Zang, 2019)), while some researchers diversify data distributions by generating virtual samples through generative adversarial networks (GANs) (Gao et al., 2020; Yang, Gu, Yin and Yang, 2020). However, according to our experiments (see Section 4), manual data augmentation and GAN-based augmentation could not consistently lead to improvements due to the inevitable deviations (Gong, Huang and Chen, 2021) between simulations and real-world underwater environments. If data augmentation pushes the supplementary data further from the true distribution, the performance of recognition models may even degrade. To address these limitations, our work presents two effective training strategies for mitigating overfitting while avoiding the risk of getting influenced by low-quality noisy samples.

First, inspired by local shift sensitivity from robust statistics (Huber, 2011), we propose smoothness-inducing regularization as an effective alternative to traditional data augmentation methods. During training, simulated noisy samples are excluded from the direct loss calculation with ground truth, but are used to compute the regularization term based on the Kullback-Leibler (KL) divergence. Since noisy samples are not directly involved in the loss calculation, the model could minimize the risk of aggravating misjudgment even if noisy samples deviate from real-world scenarios. This property makes the decision boundary of the model smoother and reduces the model sensitivity to low-quality noisy samples, thus suppressing the risk of performance degradation.

The regularization strategy mitigates overfitting by constraining model training, which can be viewed as a conservative and moderate approach. Furthermore, inspired by the success of “mixup” (Zhang, Cisse, Dauphin and Lopez-Paz, 2017) and “cutmix” (Yun, Han, Oh, Chun, Choe and Yoo, 2019) in pattern recognition tasks, we introduce a novel data augmentation strategy called local masking and replicating (LMR), which is designed specifically for time-frequency spectrogram-based recognition. LMR generates mixed spectrograms by randomly masking local patches in effective frequency bands and replicating patches in the same region from other spectrograms. Since the local regions in spectrograms contain line spectrum or modulation information within a certain time-frequency window, LMR can help the model enhance the ability to capture inter-class relationships from mixed spectrograms. This novel data augmentation strategy introduces a regularization effect

that mitigates overfitting and improves the model’s generalization to unseen data.

In this work, we thoroughly evaluate the effectiveness of our proposed methods on three underwater ship-radiated noise databases: Shipsear (Santos-Domínguez et al., 2016) (with a recognition accuracy of 83.45%), DeepShip (Irfan et al., 2021) (with a recognition accuracy of 80.05%), and a private dataset (Ren, Huang, Li, Guo and Xu, 2019) (with a recognition accuracy of 97.80%). To demonstrate the stability and robustness of our methods, we present comprehensive visualizations for further analysis. The key contributions of this work are summarized as follows:

- This work experimentally reveals the limitations of traditional data augmentation techniques that rely on the quality of simulated samples.
- We introduce a smoothness-inducing regularization strategy to alleviate overfitting and minimize the risk of performance degradation when noisy samples deviate from real-world scenarios.
- We further propose a specialized spectrogram-based data augmentation strategy - LMR, that captures inter-class relationships and improves the model’s generalization capacity.
- We point out the incomparability of existing work and release our train/test split to establish a benchmark for follow-up work.

2. Methodology

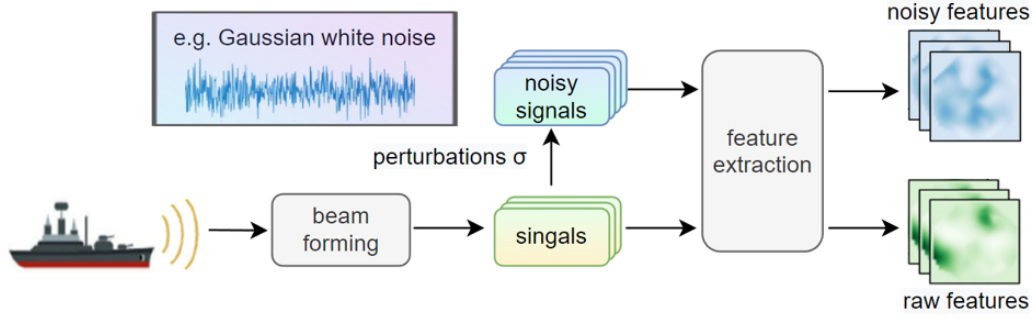
This section presents an in-depth introduction to the concepts and implementation of our proposed recognition system, which is built upon two innovative techniques: smoothness-inducing regularization, local masking and replicating.

2.1. Data Preprocessing and Feature Extraction

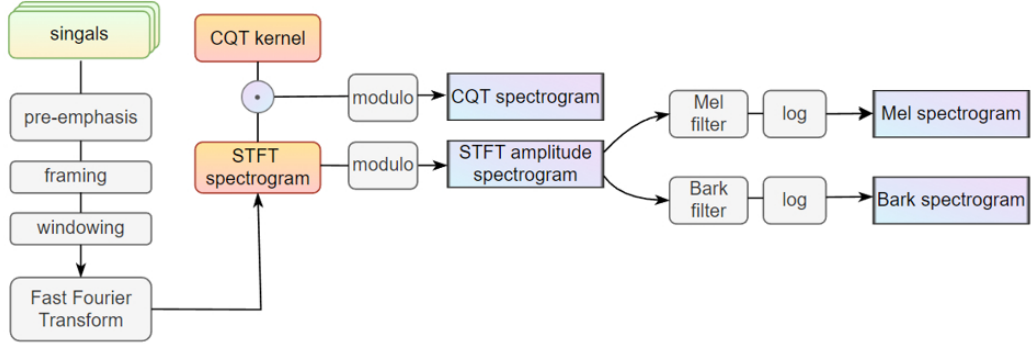
In this work, we focus on the underwater acoustic signals detected by passive sonar arrays. During the preprocessing stage, array signal processing techniques, such as beamforming, are applied to enhance the signals in target directions while suppressing interference and noise from other directions.

Figure 1(a) provides an overview of the preprocessing operations. The process begins by implementing beamforming to enhance the signals in target directions, followed by simulating possible perturbations (e.g., background noise) or building generative adversarial networks to generate noisy signals. The subsequent feature extraction process transforms all signals into acoustic features. The features derived from the original signals are referred to as “raw features”, while those obtained from the noisy signals are designated as “noisy features.”

To validate the universality of our proposed strategies, we implement four feature extraction techniques in this work. Figure 1(b) presents a detailed process of our feature



(a) The overview of the preprocessing operations. The signal radiated by the target is collected by passive sonar.



(b) Detailed steps of feature extraction. Grey boxes represent the operations and mauve boxes represent the extracted two-dimensional features.

Figure 1: The pipeline of our preprocessing process, along with the generation of noisy signals and the extraction of acoustic features.

extraction process. We begin with computing the complex FFT spectrums through framing, windowing, and short-time Fourier transform. The real component is then extracted and integrated to obtain the STFT amplitude spectrogram. Subsequently, Mel (Bark) filter banks are applied to the framed FFT spectrums for filtering, as shown in Equation (1) where f denotes frequency. Then, the filtered spectrums are converted to Mel (Bark) spectrograms using a logarithmic scale and the integrating operation.

$$\begin{aligned} Mel(f) &= 2595 \times \log\left(1 + \frac{f}{700}\right), \\ Bark(f) &= 6 \times \operatorname{arsinh}\left(\frac{f}{600}\right). \end{aligned} \quad (1)$$

Furthermore, we obtain the CQT spectrogram through the constant Q transform. We convolve the framed FFT spectrums with the CQT kernel, which is a bank of bandpass filters logarithmically spaced in frequency. Equation (2) formalizes the k -th frequency component f_k , where the octave resolution is denoted by b , and the maximum and minimum frequencies to be processed are represented by f_{max} and f_{min} , respectively.

$$CQT(f_k) = 2^{k/b} f_{min} \quad f_{min} \leq f_k \leq f_{max} \quad (2)$$

Then, the magnitude of the filtered spectrum is integrated to represent the CQT spectrogram.

2.2. Backbone Model

According to preliminary experiments (see Section 4.1), we adopt ResNet-18 with multi-head attention, an optimized convolutional neural network, as the backbone for our model. As shown in Figure 2, our backbone model consists of a 7×7 convolution layer stacked with a 3×3 max-pooling layer with a stride of 2, followed by four residual layers and an attention pooling layer. Each residual layer contains the stack of two basic block layers, each including two 3×3 convolution layers, two batch normalization layers, two ReLU layers, and a skip connection. The attention pooling layer implements a ‘‘QKV’’ (query-key-value) style multi-head attention (Wang, Girshick, Gupta and He, 2018), which assigns different weights to regions of the feature map to focus on useful information, allowing the model to learn which features are important and should be emphasized in the recognition process. Then, the outputs of multi-head attention layers are concatenated and flattened into a one-dimensional representation. Finally, we use a task-related fully-connected layer to convert the representation to prediction results.

2.3. Smoothness-inducing Regularization

We compare the traditional data augmentation method and our smoothness-inducing regularization during the training process in Figure 3. Traditional data augmentation treats both raw and noisy features as training samples, while our smoothness-inducing regularization strategy prevents noisy

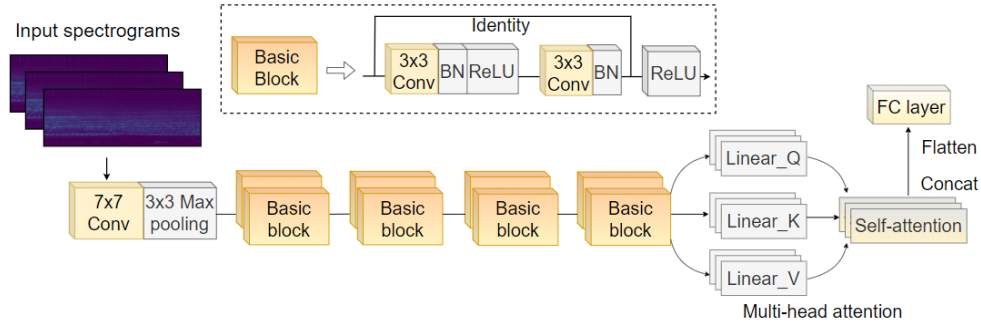


Figure 2: The structure of our backbone model: ResNet-18 with multi-head attention. “Conv” represents the convolutional layer, “BN” represents the two-dimensional batch normalization layer and “FC” represents the fully-connected layer.

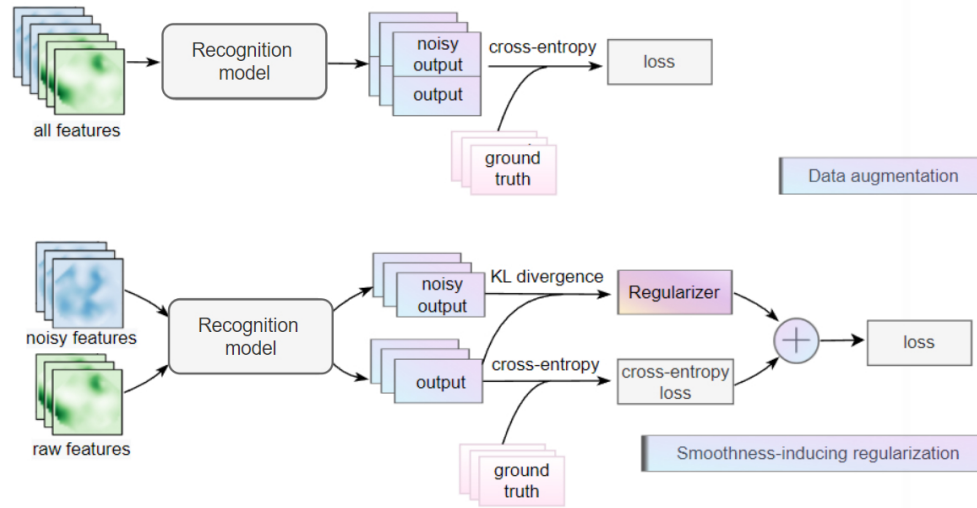


Figure 3: Comparison of the data augmentation and our smoothness-inducing regularization. For brevity, we omit the backpropagation of loss.

samples from directly contributing to the loss calculation with the ground truth. This mitigates the reliance on the quality of noisy samples and leads to a more robust training process. Our methodology is as follows:

Denote raw features as x_i , noisy features as \tilde{x}_i and corresponding labels as y_i ($i = 1, 2, \dots, n$). The model $f(\cdot)$ is fed with paired samples (x_i, y_i) and (\tilde{x}_i, y_i) simultaneously and outputs the logits $z_i = f(x_i)$ and $\tilde{z}_i = f(\tilde{x}_i)$ after forward propagation. Inspired by previous work (Jiang, He, Chen, Liu, Gao and Zhao, 2019), we apply the Kullback-Leibler (KL) divergence as the basis for the regularization term. Our optimization goal is to minimize the loss function:

$$\begin{aligned} \mathcal{L} &= \mathcal{L}_{CE}(z_i, y_i) + \alpha \mathcal{L}_{Reg}(z_i, \tilde{z}_i) \\ &= \mathcal{L}_{CE}(z_i, y_i) + \alpha (\mathcal{L}_{KL}(z_i, \tilde{z}_i) + \mathcal{L}_{KL}(\tilde{z}_i, z_i)), \end{aligned} \quad (3)$$

where \mathcal{L}_{CE} represents the cross-entropy loss, and the weight coefficient α serves to adjust the weight of the regularization term, thus controlling the impact of smoothness-inducing regularization on the recognition model. We could set $\alpha = 0$ to deactivate the smoothness-inducing regularization when it is not needed. The selection of the value of α can be found in Section 4.4.

\mathcal{L}_{Reg} represents the regularization term based on KL divergence. KL divergence measures the “distance” between two discrete probability distributions. We feed the logits z_i and \tilde{z}_i into the softmax function and get the normalized probability distribution p_i and \tilde{p}_i . The KL divergence-based term \mathcal{L}_{KL} can be formulated as:

$$\mathcal{L}_{KL}(z_i, \tilde{z}_i) = \mathcal{D}_{KL}(p_i \| \tilde{p}_i) = \frac{1}{n} \sum_{i=1}^n p_i \log \frac{p_i}{\tilde{p}_i}, \quad (4)$$

where $\mathcal{D}_{KL}(p_i \| \tilde{p}_i)$ represents the KL divergence between p_i and \tilde{p}_i . The regularization term in Equation (4) is minimized when the model does not significantly change predictions for perturbed samples ($p_i \approx \tilde{p}_i$). It reduces local sensitivity by encouraging similarity between the predictions for x_i and its neighbors \tilde{x}_i , thus achieving a smoother decision boundary. This smoothness-inducing property can help improve the robustness of recognition models by reducing the sensitivity to noisy perturbations, contributing to consistent and reliable model performance.

2.4. Local Masking and Replicating

To further alleviate the overfitting problem and enhance the model’s generalization ability, we propose a novel data

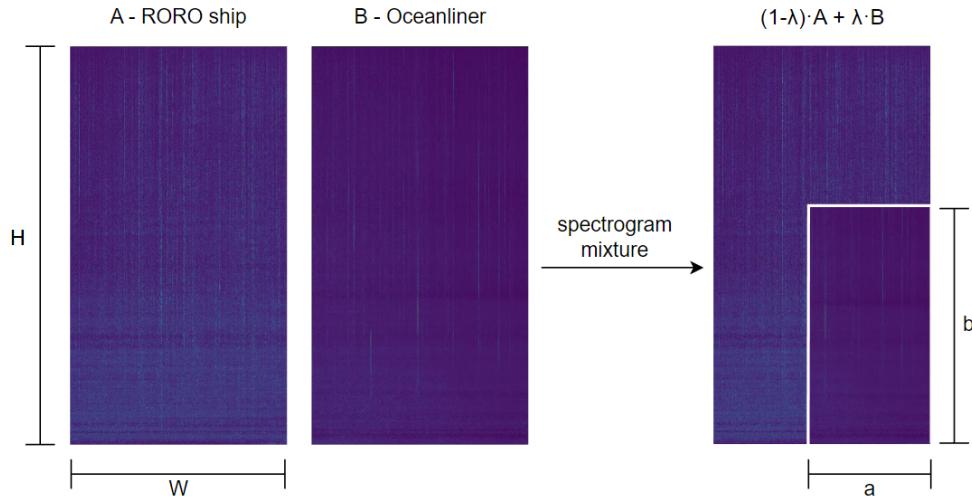


Figure 4: An example for local masking and replicating (LMR). The samples in the figure are selected from two 30-second segments in Shipsear.

augmentation strategy called local masking and replicating (LMR) that specializes in diversifying the distribution of training data for time-frequency spectrogram-based recognition. This technique is universally applicable and generates new training samples solely based on the raw data, eliminating the need for manual perturbations or adversarial samples.

LMR is applied exclusively during the training phase. Before the training process, we analyze the effective frequency bands of signals and obtain input spectrograms with lower information redundancy by limiting the frequency bands. As depicted in Figure 4, LMR randomly samples two input spectrograms of any category in the batch during training. One spectrogram randomly masks local patches, while patches of the same size and position from another spectrogram are replicated and inserted in the masked area of the former spectrogram. The mixed “spectrogram” serves as the input sample for training. We denote the width and height of input spectrograms as W and H , respectively, and represent the removed region as an $a \times b$ patch where $a(a \in (0, W))$ and $b(b \in (0, H))$ represent the width and height of the masked and replicated regions. a and b are random values within their value range, which change dynamically with sampling. We denote the two sampled spectrograms and the mixed “spectrogram” as $x_i, x_j, \mathcal{X}_{ij}$, respectively. The model $f(\cdot)$ takes \mathcal{X}_{ij} as input and outputs $\mathcal{Z}_{ij} = f(\mathcal{X}_{ij})$ after feedforward. The coefficient λ measures the proportion of mixture, where $\lambda = 1 - \frac{a \cdot b}{H \cdot W}$. The corresponding loss is formulated as:

$$\mathcal{L}_{LMR} = \lambda \mathcal{L}_{ce}(\mathcal{Z}_{ij}, y_i) + (1 - \lambda) \mathcal{L}_{ce}(\mathcal{Z}_{ij}, y_j), \quad (5)$$

where \mathcal{L}_{ce} denotes the cross-entropy loss. Notably, when LMR is activated, \mathcal{L}_{LMR} will replace \mathcal{L}_{CE} in Equation (3). Since the local regions in spectrograms contain line spectrum or modulation information within a certain time-frequency window, the mixed spectrograms \mathcal{X}_{ij} may contain distinguishable features from different categories. The

model can enhance the ability to capture inter-class relationships by directly learning from mixed spectrograms, thereby better distinguishing similar categories.

In addition, we activate LMR dynamically and intermittently during training. Each batch has a 50% probability of being directly fed to the model (deactivate LMR), and a 50% probability of implementing sampling and LMR operations. In this way, each sample has the opportunity to directly serve as input or participate in LMR. Compared with always activating LMR, this strategy can reduce computational consumption while diversifying the training inputs.

2.5. Optimization objective

When both of our proposed strategies are activated, our optimization objective can be represented as minimizing the loss function as follows:

$$\begin{aligned} \mathcal{L} &= \mathcal{L}_{LMR} + \alpha \mathcal{L}_{Reg} \\ &= \mathcal{L}_{LMR} + \alpha [\mathcal{L}_{KL}(z_i, \tilde{z}_i) + \mathcal{L}_{KL}(\tilde{z}_i, z_i)] \\ &= \lambda \mathcal{L}_{ce}(\mathcal{Z}_{ij}, y_i) + (1 - \lambda) \mathcal{L}_{ce}(\mathcal{Z}_{ij}, y_j) + \\ &\quad \alpha \left[\frac{1}{n} \left(\sum_{i=1}^n p_i \log \frac{p_i}{\tilde{p}_i} + \sum_{i=1}^n \tilde{p}_i \log \frac{\tilde{p}_i}{p_i} \right) \right]. \end{aligned} \quad (6)$$

To minimize the optimization objective, the model should accurately capture the distinguishable characteristics of different classes while being insensitive to perturbations.

3. Experiment Setup

3.1. Datasets

In this work, we use three underwater ship-radiated noise datasets across different scales. The detailed information is presented in the subsequent paragraphs:

1. Shipsear (Santos-Domínguez et al., 2016) is an open-source database of underwater recordings of ship and boat sounds. It currently comprises 90 records representing sounds

Table 1

Number of samples (30-second segments) in the training, validation, test set for the three datasets.

Split	Shipsear	DTIL	DeepShip
Training	400	1655	6742
Validation	71	292	1190
Test	116	354	2547
Total	587	2301	10479

from 11 vessel types, consisting of nearly 3 hours of recordings. To ensure sufficient data for the “train, validation, test” split, we select a subset of 9 categories (dredger, fish boat, motorboat, mussel boat, natural noise, ocean liner, passenger ship, ro-ro ship, and sailboat) for the recognition task.

2. DeepShip (Irfan et al., 2021) is an open-source underwater acoustic benchmark dataset, which consists of 47.07 hours of real-world underwater recordings of 265 different ships belonging to four classes (cargo, passenger ship, tanker, and tug).

3. Our private dataset (Ren et al., 2019)- DTIL is a dataset collected from Thousand Island Lake, which contains multiple sources of interference. The dataset comprises 330 minutes of the speedboat and 285 minutes of the experimental vessel.

3.2. Division of data

In this work, we divide each signal into 30-second segments with a 15-second overlap. To prevent information leakage, we make sure that segments in the training set and the test set must not belong to the same audio track. This ensures that the reported accuracy reflects the recognition ability and generalization performance, rather than the memory capacity.

We note that many previous works on underwater acoustic recognition tasks do not provide their training/test split, which makes it challenging to make a fair comparison. Therefore, we release our carefully selected train/test split of Shipsear and DeepShip in Appendix B. During training, we randomly take 15% of the data in the training set as the validation set. We hope that it could serve as a reliable benchmark for subsequent work pursuing fair comparisons. Table 1 displays the number of samples (30-second segments) in the training, validation, and test set for the three datasets.

3.3. Effective frequency bands

The energy of the target signals primarily concentrates on specific frequency ranges. To facilitate the replicated area in LMR containing valid information, we take the effective frequency band as a replacement for the full-frequency band during analyzing underwater signals. Moreover, time-frequency transformation within the bandwidth could reduce the redundancy of acoustic features, thus enhancing recognition performance while reducing time and hardware consumption. The distribution of energy in target signals

varies across different frequency bands for the three datasets, so we set different effective frequency bands for each (see Table 2). Details regarding the effective frequency band selection could be found in Appendix A. Notably, according to the Nyquist theory, the upper limit of the effective frequency band must be less than half of the sample rate.

3.4. Parameters Setup

Regarding framing, we conduct experiments to investigate the effect of frame length on recognition results, which is shown in Appendix C. In this work, we set the frame length as 50ms and the frame shift as 25ms. Furthermore, we set the number of Mel or Bark filter banks to 300 as default. For the CQT kernel, we set the octave resolution to 30 and set the maximum(minimum) frequency according to the boundary of effective frequency band for each dataset. When extracting the CQT spectrogram, we set the time resolution to 30 as default. The dimensions of the various acoustic features are shown in Table 2.

During training, we employ the AdamW (Loshchilov and Hutter, 2017) optimizer. We set the learning rate to $5e-4$, batch size to 64, and weight decay to $1e-5$ for all experiments. All models are trained for 100 epochs on a single A40 GPU.

4. Results and analysis

For the multi-class recognition problem addressed in this work, we uniformly adopt the accuracy rate as the evaluation metric. The accuracy rate is calculated by dividing the number of correct predictions by the total number of predictions. It provides an intuitive measure of the model’s ability to distinguish between different classes accurately. Besides, since the number of complete audio files in the test set is limited, several groups of experiments yield the same file-level accuracy. Therefore, we report results at the segment level (30 seconds) rather than the file level.

In this section, we validate the effectiveness of our proposed methods on three datasets and conduct detailed comparison experiments to separately verify the gains brought by smoothness-inducing regularization and LMR. To better demonstrate the superiority of our proposed methods, we visualize our results by confusion matrix heat map and gradient-weighted class activation mapping (CAM) (Selvaraju, Cogswell, Das, Vedantam, Parikh and Batra, 2017). An introduction to the concept of the confusion matrix heat map and CAM can be seen in Section 4.2.

4.1. Main results

First, we conduct preliminary experiments on the model backbone (see the top part of Table 3). To ensure a fair comparison, we uniformly use the STFT spectrogram without any augmentation and regularization. We implement several baselines (Howard, Sandler, Chu, Chen, Chen, Tan, Wang, Zhu, Pang, Vasudevan et al., 2019; He, Zhang, Ren and Sun, 2016; Hu, Shen and Sun, 2018) that perform well in underwater acoustics and observe that the ResNet-based

Table 2

Information of the three datasets and corresponding feature dimensions. “SR” represents the sampling rate and “Dim” represents the dimension of features.

Dataset	Duration (hours)	SR (Hz)	Efficient band (Hz)	STFT Dim	Mel/Bark Dim	CQT Dim
Shipsear	2.94	52734	100-26367	1199,1318	1199,300	899,340
DTIL	10.25	17067	100-2000	1199,100	1199,300	899,229
Deepship	47.07	32000	100-8000	1199,400	1199,300	899,289

Table 3

Main results across various datasets and features. “smooth reg” represents smoothness-inducing regularization for short. The underlined part indicates a decrease in performance compared to the baseline.

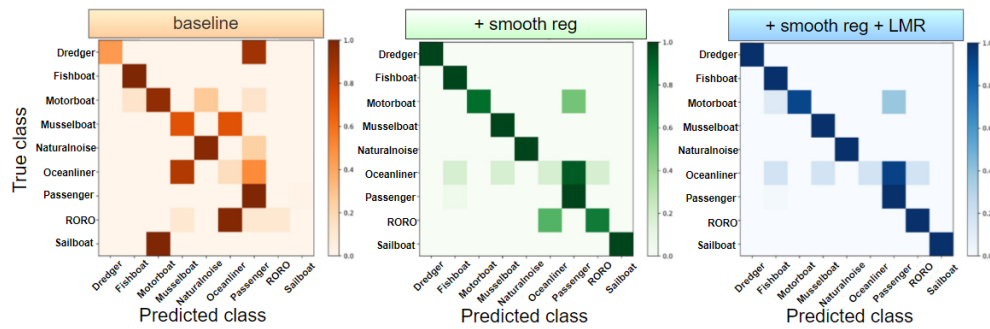
Model	Features	Methods	Shipsear	DTIL	DeepShip
Random forest (RF)	STFT spec	-	59.33	82.56	66.71
Support vector machines (SVM)	STFT spec	-	65.65	88.74	69.24
FCN(1-d convolution)	STFT spec	-	72.56	91.67	72.98
MobileNet-v3 small	STFT spec	-	70.02	90.54	70.45
ResNet-18	STFT spec	-	75.16	94.98	74.02
SE-ResNet-18	STFT spec	-	71.59	92.25	71.36
ResNet-18+linear attention	STFT spec	-	74.99	95.61	74.59
ResNet-18+multi-head attention	STFT spec	-	75.24	95.93	74.68
ResNet-18+multi-head attention	STFT spec	-	75.24	95.93	74.68
		+noise aug	78.45	96.05	75.07
		+GANs aug	76.05	96.14	75.98
		+smooth reg (noise)	81.90	97.74	76.38
		+LMR	82.76	96.61	78.40
		+smooth reg, LMR	82.97	97.80	78.56
ResNet-18+multi-head attention	Mel spec	-	77.14	95.48	74.85
		+noise aug	78.72	95.58	75.27
		+GANs aug	79.68	<u>95.45</u>	75.79
		+smooth reg (noise)	82.76	95.76	77.05
		+LMR	82.76	96.33	75.38
		+smooth reg, LMR	83.45	96.50	77.12
ResNet-18+multi-head attention	Bark spec	-	72.86	96.30	75.15
		+noise aug	75.86	96.33	<u>74.18</u>
		+GANs aug	74.59	96.65	<u>75.08</u>
		+smooth reg (noise)	77.72	96.76	75.75
		+LMR	79.31	96.61	77.46
		+smooth reg, LMR	79.25	96.93	77.80
ResNet-18+multi-head attention	CQT spec	-	73.33	96.48	77.82
		+noise aug	74.41	97.18	77.86
		+GANs aug	74.43	96.89	<u>77.12</u>
		+smooth reg (noise)	75.86	97.18	78.25
		+LMR	81.03	97.18	78.97
		+smooth reg, LMR	82.76	97.56	80.05

model has significant performance advantages over traditional methods (RF, SVM) and other convolutional neural networks (FCN, MobileNet). Among them, ResNet with multi-head attention achieves the best recognition accuracy on the three datasets. The application of multi-head attention mechanism allows the model to flexibly focus on effective information and avoid being influenced by redundant parts. Given its superior and stable performance, we choose ResNet with multi-head attention as the unified model backbone for all experiments in this work. A detailed description of model structures is available in Section 2.2 and Appendix D.

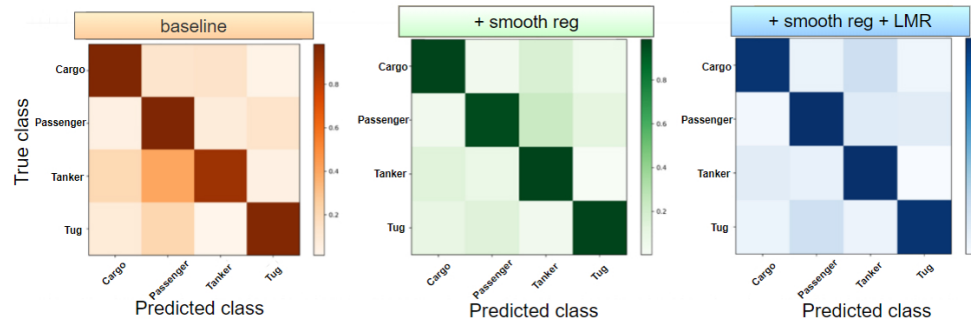
We then focus on the comparison experiments between various data augmentation and regularization strategies (see

the bottom part of Table 3). We implement two data augmentation strategies as the baseline methods: adding Gaussian white noise with the signal-to-noise ratio of 5-30dB (noise aug), and generating adversarial samples with vanilla GAN (GANs aug). To enable a fair comparison, when implementing smoothness-inducing regularization, we copy the parameter settings of “noise aug” to generate the same noisy samples. To avoid the influence of the amount of training data on the results, we ensure that all three augmentation strategies generate noisy samples equal in number to raw training samples. That is, the number of total training samples is doubled after augmentation.

As depicted in Table 3, we find that classic data augmentation methods cannot consistently bring boosts and sometimes even have a negative effect (see the underlined results



(a) Confusion matrix heat maps for Shipsear. There are nine categories: dredger, fish boat, motorboat, mussel boat, natural noise, ocean liner, passenger ship, ro-ro ship and sailboat.



(b) Confusion matrix heat maps for DeepShip. There are four categories: cargo, passenger ship, tanker, tug.

Figure 5: Confusion matrix heat map for two datasets. The three subplots represent: 1. baseline; 2. with smooth reg; 3. with smooth reg and LMR. “smooth reg” represents smoothness-inducing regularization for short.

in Table 3). Especially for the model based on Bark spectrogram on Deepship, the employment of “noise aug” reduces the recognition accuracy by 0.97%. It shows that recognition models face the risk of performance degradation when noisy samples deviate from real-world scenarios. Models may learn biases from low-quality samples if they treat manually added perturbations as the inherent property of ship-radiated noise. Compared to classic data augmentation methods, our proposed regularization strategy consistently brings promising and stable improvement with minimal risk of performance degradation. As a regularization method, it avoids noisy samples from directly participating in model training, resulting in less negative impact.

Moreover, LMR achieves surprising results on all datasets. The performance gains from LMR sometimes even outweigh the gains obtained by smoothness-inducing regularization. Especially on Shipsear, LMR can bring 5.62% ~ 7.70% accuracy improvement to models based on different features. It highlights the efficacy of constructing mixed samples to capture inter-class relationships during training. We also observe that the combination of smoothness-inducing regularization and LMR can further improve performance, indicating good compatibility between the two strategies.

4.2. Visualization

This subsection aims to provide a visual representation of the results to facilitate comprehension and interpretation.

We present the confusion matrix heat map for the recognition results and use the gradients in back-propagation as weights to draw the class activation mapping.

The confusion matrix compares the true labels (vertical axis) to the predicted labels (horizontal axis), and the confusion matrix heat map (see Figure 5) is the graphical representation of the confusion matrix, where the values in the matrix are represented as colors. The color scale used in a heatmap ranges from light (representing low values) to dark (representing high values). Figure 5 shows that our proposed strategies improve the recognition accuracy of all categories. Take the results on Shipsear as an example, the baseline method often misclassifies dredgers, ocean liners, ro-ro ships, and completely fails to identify sailboats. After applying our smoothness-inducing regularization and LMR augmentation, the recognition accuracy for dredgers, ro-ro ships, and sailboats reaches 100%, which is a very satisfactory improvement.

Then, we generate the class activation mapping (CAM) by using the gradients in back-propagation as weights. The CAM is a graphical representation of the input spectrograms, with color indicating the impact of a region on the network’s decision. Dark colors indicate a crucial role in the decision-making process. The CAM heat map faithfully highlights important regions in spectrograms for deep model prediction in recognition tasks. By analyzing the CAM in Figure 6, we observe that our proposed optimizations enable models to emphasize global information, thus avoiding bias towards specific local information (e.g., see the CAM for

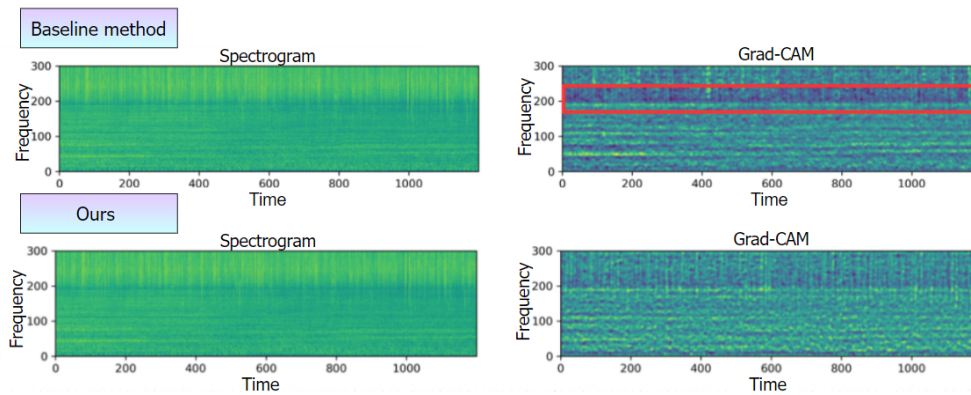


Figure 6: The Mel spectrogram and the corresponding CAM heat map for the baseline (top) and our method (bottom). We take the 30-second segment of a ro-ro ship in Shipsear as the example.

Table 4

Performance of Mel-spectrogram-based models on the test set with different SNRs. We do not employ LMR to control interference factors.

Method	Range of SNR	Shipsear	DTIL	DeepShip
Noise augmentation	-	78.72	95.58	75.27
	5 ~ 30	78.52	95.50	75.19
	-5 ~ 20	76.05	94.46	73.36
	-15 ~ 10	71.69	92.45	68.67
smoothness-inducing regularization (noise)	-	82.76	95.76	77.05
	5 ~ 30	82.66	95.63	77.01
	-5 ~ 20	81.95	94.78	76.66
	-15 ~ 10	79.69	93.70	73.03

the baseline model in Figure 6, where the vertical scale is 200.). The avoidance of local bias can enhance recognition performance.

In addition, we display the four spectrogram-based features along with their corresponding CAM heat map in Appendix E. Our purpose is to show the critical components of different features that influence network decisions.

4.3. Sensitivity to perturbations

In this set of experiments, we add white Gaussian noise with different signal-to-noise ratios (SNRs) to the test data. A lower SNR indicates a larger magnitude of the noise perturbation. We use trained models (as mentioned above, trained with 5~30dB noise perturbations) to evaluate the test data with different SNRs. We aim at exploring whether models based on smoothness-inducing regularization are less sensitive to perturbations. As illustrated in Table 4, the model trained with manual noise augmentation maintains a performance drop of less than 3% when the SNR of the test data is not lower than -5dB, whereas the recognition accuracy sharply decreases by 7.03% when tested on data with -15~10dB SNR. By contrast, the model based on smoothness-inducing regularization exhibits consistent performance even under substantial perturbations. When the SNR of the test data reaches -15dB, the performance of our model only drops by 3.07%, and the recognition accuracy remains at approximately 80%. Our model can benefit from the smoother decision boundary brought about by the regularization strategy. Therefore, we conclude that

Table 5

Experiments with different regularization coefficient α across various acoustic features. We do not employ LMR to control interference factors.

Features	α	Shipsear	DTIL	DeepShip
STFT spec	0	75.24	95.93	74.68
	0.5	81.90	97.18	75.83
	1	81.47	97.05	75.52
	2	78.45	97.74	76.38
Mel spec	0	77.14	95.48	74.85
	0.5	81.14	95.76	77.05
	1	81.41	95.48	75.79
	2	82.76	95.20	75.13
Bark spec	0	72.86	96.30	75.15
	0.5	77.72	96.48	75.40
	1	76.28	96.76	75.75
	2	76.00	96.20	74.93
CQT spec	0	73.33	96.48	77.82
	0.5	75.28	97.18	77.86
	1	75.86	96.89	78.17
	2	75.41	96.61	78.25

models employing smoothness-inducing regularization are less sensitive to perturbations and can exhibit superior robustness against perturbations.

4.4. Selection of regularization coefficient

In this subsection, our focus is on selecting the appropriate regularization coefficient α . As shown in Table 5,

Table 6

Comparison experiments on LMR and mixup. The underlined part indicates a decrease in performance compared to the baseline. We do not employ regularization to control interference factors.

Features	Augmentation	Shipsear	DTIL	DeepShip
STFT spec	-	75.24	95.93	74.68
	mixup	79.31	95.76	74.83
	LMR	82.76	96.61	78.40
Mel spec	-	77.14	95.48	74.85
	mixup	<u>76.72</u>	96.05	75.42
	LMR	82.76	96.33	75.38
Bark speck	-	72.86	96.30	75.15
	mixup	75.86	96.51	<u>73.77</u>
	LMR	79.31	96.61	77.46
CQT spec	-	73.33	96.48	77.82
	mixup	79.31	97.18	78.48
	LMR	81.03	97.18	78.97

the value of α has a noticeable impact on the results. Taking the model based on STFT features on shipsear as an example, setting α as 0.5 achieves a recognition accuracy rate of 81.90%. By contrast, setting α as 2 can only get an accuracy rate of 78.45%, with a gap of 3.45%. Therefore, it is important to set a suitable α to make the smoothness-inducing regularization reach the best performance for different databases and acoustic features. If α is set too low, the regularization constraint is insufficient, and the model may still suffer from overfitting. Conversely, if α is set too high, the regularization may become overly aggressive and impede model learning. Typically, selecting α from the range of 0.5, 1, or 2 yields favorable outcomes. When confronted with diverse data and features, it is necessary to experiment with different values to obtain the optimal α .

4.5. Capture inter-class relationships: LMR vs mixup

For pattern recognition tasks, mixup (Zhang et al., 2017) is a popular data augmentation technique that can capture inter-class relationships. It performs a linear mixture operation between the input and its corresponding label to generate virtual input samples. In this set of experiments, we implement comparison experiments between LMR and mixup. As indicated by the results in Table 6, LMR provides greater gains for models based on four different acoustic features. Notably, on the data-scarce Shipsear dataset, LMR improves accuracy by 2.86%~9.04%. Additionally, we observe that LMR is more stable in most cases. Mixup may cause a slight accuracy drop (see the underlined results in Table 6), whereas LMR does not show any risk of performance degradation in our experiments.

According to our analysis, since the stripes in the spectrogram contain line spectrum and periodic modulation information, mixing them linearly may result in aliasing or distortion, thus hurting the performance. The aliasing of the line spectrum or periodic stripes may cause a shift in the signal's frequency or period. Therefore, we argue that "mixup" is not ideal for spectrogram-based acoustic recognition. Conversely, our proposed LMR is specially

designed for spectrogram-based recognition. Regions from different spectrograms are strictly kept separate to prevent aliasing. LMR enables virtual samples to capture inter-category relationships without the risk of aliasing, making it a more suitable approach for spectrogram-based acoustic recognition.

5. Conclusion

Through our experimental investigations, we have uncovered the limitations of traditional data augmentation techniques that heavily rely on signal quality and augmentation methods. Based on the observation, we propose innovative regularization and augmentation techniques that are less reliant on the quality of noisy samples. Our proposed smoothness-inducing regularization allows models to learn robust knowledge from noisy samples while minimizing biases toward low-quality supplementary training samples. Additionally, we introduce a specialized spectrogram-based augmentation strategy, called local masking and replicating, which enhances the diversity of the training data distribution and captures inter-class relationships between samples. Through comprehensive experiments and visual analyses, we demonstrate the effectiveness of our proposed techniques.

However, our experiments also reveal certain limitations of our proposed methods. First, while smoothness-inducing regularization performs well on the data-scarce Shipsear dataset, it only provides limited improvements when applied to the data-abundant DeepShip dataset. This indicates that the regularization technique can only mitigate the overfitting problem, rather than enhance the model's performance upper bound. Furthermore, the application scenarios of LMR are relatively limited. Despite its efficacy in spectrogram-based multi-class recognition, LMR can sometimes have negative effects on other tasks, such as detection tasks.

Acknowledgements

This research is supported by the IOA Frontier Exploration Project (No. ZYTS202001) and Youth Innovation Promotion Association CAS.

Appendix

A. Selection of effective frequency bands

Table 7 presents the recognition results obtained using different frequency bands. The input feature for all experiments is the STFT spectrogram, and the model backbone for all experiments is ResNet with multi-head attention. No regularization or augmentation technique is applied. The frequency band with the best performance is selected as the effective frequency band for the three databases, as shown in Table 2.

B. Train/Test split for Shipsear and DeepShip

We find that almost all previous works on underwater acoustic recognition tasks do not release their split of

Table 7

Selection of effective frequency bands. The upper limit of their effective frequency bands varies due to the different sampling rates.

frequency bands(Hz)	Shipsear	DTIL	DeepShip
100-2k	-	95.93	-
100-4k	-	95.08	74.37
100-8k	60.69	94.52	74.68
100-12k	64.14	-	74.53
100-16k	70.90	-	73.66
100-24k	74.34	-	-
100-26.367k	75.24	-	-

Table 8

Train/Test split for Shipsear. The "ID" in the table refers to the ID of the .wav file in the dataset.

Category	ID in Training set	ID in Test set
dredger	80,93,94,96	95
fish boat	73,74,76	75
motorboat	21,26,33,39,45,51,52,70,77,79	27,50,72
mussel boat	46,47,49,66	48
natural noise	81,82,84,85,86,88,90,91	83,87,92
ocean liner	16,22,23,25,69	24,71
passenger ship	06,07,08,10,11,12,14,17,32,34,36,38,40,41,43,54,59,60,61,63,64,67	9,13,35,42,55,62,65
ro-ro ship	18,19,58	20,78
sailboat	37,56,68	57

Table 9

Train/Test split for DeepShip. The "ID" in the table refers to the ID of the .wav file in the dataset.

Category	ID in Training set	ID in Test set
cargo	Else	01,02,04,05,18,30,32,35,40,48,56,62,63,67,68,72,74,79,83,91,92,93,95,97,100,104
passenger ship	Else	02,04,05,07,11,15,17,19,20,23,30,31,37,45,46,52,53,60,61,62,64,67,68,70,75,76,77,84,86,91,101,106,113,117,122,125,129,130,134,135,142,144,152,157,159,161,167,168,177,179,187,188,189
tanker	Else	02,03,04,07,08,13,14,15,19,22,25,28,35,37,46,58,62,71,73,79,82,84,88,89,92,99,106,115,118,124,126,127,131,134,141,144,147,151,153,156,158,167,171,178,179,185,186,190,192,193,201,205,213,217,228,233
tug	Else	07,08,18,20,24,25,27,29,32,33,37,39,40,44,45,56,59,70

train/test sets, which makes it challenging to make a fair comparison. In this work, we release our carefully selected train/test split of Shipsear and DeepShip (see Table 8, 9). We believe that it could serve as a reliable benchmark for subsequent work pursuing fair comparisons³.

C. The relationship between frame length and recognition results

Table 10 shows the recognition results obtained using different frame lengths. The input feature for all experiments is the STFT spectrogram, and the model backbone for all experiments is ResNet with multi-head attention. No regularization or augmentation technique is applied. The results

³The train-test split for Shipsear is also released at <https://github.com/xy980523/ShipsEar-An-Unofficial-Train-Test-Split>

Table 10

The relationship between frame length and recognition results.

Frame length/Frame shift	Shipsear	DTIL	DeepShip
30ms/15ms	72.78	95.10	73.48
50ms/25ms	75.24	95.93	74.68
100ms/50ms	72.78	95.77	74.25
150ms/75ms	74.56	95.31	71.97

indicate that setting the frame length to 50ms is the optimal choice for all three databases.

D. Network Parameters and Training Time Cost

In this work, we implement several baselines that are widely applied in underwater acoustic target recognition tasks, including random forest, support vector machines, fully convolution networks, Mobilenet-v3 small (Howard et al., 2019), ResNet-18 (He et al., 2016), SE-ResNet-18 (Hu et al., 2018) and ResNet-18 with attention mechanism.

Two classic machine learning methods are implemented as weak baselines: random forest, which is an ensemble learning method that uses multiple decision trees to make predictions, and support vector machines, which are a type of classification model that navigates data by maximizing the margin between different classes. In addition, we implement several methods based on deep neural networks. Fully convolutional networks (FCN) with 1-d convolution employ three one-dimensional convolution layers with different convolution kernel sizes (8×8, 5×5, 3×3). MobileNet-v3 small employs techniques such as depth-wise separable convolutions, which replace a standard convolution with a depth-wise convolution and a point-wise convolution. ResNet consists of a 7×7 convolutional layer, a 3×3 max pooling layer, four basic blocks (see Figure 2), an adaptive average pooling layer, and a fully-connected layer. SE-ResNet is a ResNet-style model that includes a squeeze-and-excitation (SE) mechanism designed to improve the quality of the output feature maps. ResNet with multi-head attention is detailedly introduced in Section 2.2. The number of parameters and training time cost on Shipsear is illustrated in Table 11.

E. Class Activation Mapping for four spectrogram-based features

This work is based on four spectrogram-based acoustic features. In Appendix E, we use a 30-second segment (belonging to ro-ro ship) in Shipsear to exemplify the STFT, Mel, Bark, CQT spectrograms, and their corresponding class activation mappings, as shown in Figure 7. We utilize CAMs to highlight important regions in spectrograms, which is conducive to exploring which parts of the features play a crucial role in recognition.

Table 11

The number of parameters and training time cost on Shippsear.

Model	Methods	Para num(MB)	Time cost(mins)
FCN(1-d convolution)	-	0.545	3.9
MobileNet-v3 small	-	2.425	9.5
ResNet-18	-	10.657	26.4
SE-ResNet-18	-	7.234	24.8
ResNet-18+linear attention	-	11.149	27.0
ResNet-18+multi-head attention	-	11.841	27.6
	+noise aug	11.841	48.0
	+GANs aug	11.841	97.8
	+smooth reg	11.841	47.6
	+LMR	11.841	28.0
	+smooth reg, LMR	11.841	49.5

CRedit authorship contribution statement

Ji Xu: Conceptualization, Resources, Writing - Original Draft, Writing - Review & Editing, Supervision, Project administration, Funding acquisition. **Yuan Xie:** Methodology, Software, Validation, Formal analysis, Investigation, Data Curation, Writing - Original Draft, Writing - Review & Editing, Visualization. **Wenchao Wang:** Methodology, Investigation, Data Curation, Supervision.

References

- Brooker, A., Humphrey, V., 2016. Measurement of radiated underwater noise from a small research vessel in shallow water. *Ocean Engineering* 120, 182–189.
- Chen, J., Han, B., Ma, X., Zhang, J., 2021. Underwater target recognition based on multi-decision lofar spectrum enhancement: A deep-learning approach. *Future Internet* 13, 265.
- Courmontagne, P., Ouelha, S., Chaillan, F., 2012. On time-frequency representations for underwater acoustic signal, in: 2012 Oceans, IEEE. pp. 1–9.
- Das, A., Kumar, A., Bahl, R., 2013. Marine vessel classification based on passive sonar data: The cepstrum-based approach. *IET Radar, Sonar & Navigation* 7, 87–93.
- Fillinger, L., de Theije, P., Zampolli, M., Sutin, A., Salloum, H., Sedunov, N., Sedunov, A., 2010. Towards a passive acoustic underwater system for protecting harbours against intruders, in: 2010 International WaterSide Security Conference, IEEE. pp. 1–7.
- Gao, Y., Chen, Y., Wang, F., He, Y., 2020. Recognition method for underwater acoustic target based on dcgan and densenet, in: 2020 IEEE 5th International Conference on Image, Vision and Computing (ICIVC), IEEE. pp. 215–221.
- Gong, Y., Huang, L., Chen, L., 2021. Eliminate deviation with deviation for data augmentation and a general multi-modal data learning method. *arXiv preprint arXiv:2101.08533*.
- He, K., Zhang, X., Ren, S., Sun, J., 2016. Deep residual learning for image recognition, in: Proceedings of the IEEE conference on computer vision and pattern recognition, pp. 770–778.
- Howard, A., Sandler, M., Chu, G., Chen, L.C., Chen, B., Tan, M., Wang, W., Zhu, Y., Pang, R., Vasudevan, V., et al., 2019. Searching for mobilenetv3, in: Proceedings of the IEEE/CVF international conference on computer vision, pp. 1314–1324.
- Hu, J., Shen, L., Sun, G., 2018. Squeeze-and-excitation networks, in: Proceedings of the IEEE conference on computer vision and pattern recognition, pp. 7132–7141.
- Huang, H., Zhou, H., Yang, X., Zhang, L., Qi, L., Zang, A.Y., 2019. Faster r-cnn for marine organisms detection and recognition using data augmentation. *Neurocomputing* 337, 372–384.
- Huber, P.J., 2011. Robust statistics, in: International encyclopedia of statistical science. Springer, pp. 1248–1251.
- Irfan, M., Jiangbin, Z., Ali, S., Iqbal, M., Masood, Z., Hamid, U., 2021. Deepship: An underwater acoustic benchmark dataset and a separable convolution based autoencoder for classification. *Expert Systems with Applications* 183, 115270.
- Jiang, H., He, P., Chen, W., Liu, X., Gao, J., Zhao, T., 2019. Smart: Robust and efficient fine-tuning for pre-trained natural language models through principled regularized optimization. *arXiv preprint arXiv:1911.03437*.
- Ke, X., Yuan, F., Cheng, E., 2020. Integrated optimization of underwater acoustic ship-radiated noise recognition based on two-dimensional feature fusion. *Applied Acoustics* 159, 107057.
- Krizhevsky, A., Sutskever, I., Hinton, G.E., 2012. Imagenet classification with deep convolutional neural networks. *Advances in neural information processing systems* 25.
- LeCun, Y., Bengio, Y., Hinton, G., 2015. Deep learning. *nature* 521, 436–444.
- Li, Y., Li, Y., Chen, X., Yu, J., 2017. Denoising and feature extraction algorithms using npe combined with vmd and their applications in ship-radiated noise. *Symmetry* 9, 256.
- Liu, F., Shen, T., Luo, Z., Zhao, D., Guo, S., 2021. Underwater target recognition using convolutional recurrent neural networks with 3-d mel-spectrogram and data augmentation. *Applied Acoustics* 178, 107989.
- Loshchilov, I., Hutter, F., 2017. Decoupled weight decay regularization. *arXiv preprint arXiv:1711.05101*.
- Ren, J., Huang, Z., Li, C., Guo, X., Xu, J., 2019. Feature analysis of passive underwater targets recognition based on deep neural network, in: OCEANS 2019-Marseille, IEEE. pp. 1–5.
- Ren, J., Xie, Y., Zhang, X., Xu, J., 2022. Ualf: A learnable front-end for intelligent underwater acoustic classification system. *Ocean Engineering* 264, 112394.
- Santos-Domínguez, D., Torres-Guijarro, S., Cardenal-López, A., Pena-Gimenez, A., 2016. Shippsear: An underwater vessel noise database. *Applied Acoustics* 113, 64–69.
- Selvaraju, R.R., Cogswell, M., Das, A., Vedantam, R., Parikh, D., Batra, D., 2017. Grad-cam: Visual explanations from deep networks via gradient-based localization, in: Proceedings of the IEEE international conference on computer vision, pp. 618–626.
- Wang, S., Zeng, X., 2014. Robust underwater noise targets classification using auditory inspired time-frequency analysis. *Applied Acoustics* 78, 68–76.
- Wang, X., Girshick, R., Gupta, A., He, K., 2018. Non-local neural networks, in: Proceedings of the IEEE conference on computer vision and pattern recognition, pp. 7794–7803.
- Xie, Y., Ren, J., Xu, J., 2022a. Adaptive ship-radiated noise recognition with learnable fine-grained wavelet transform. *Ocean Engineering* 265, 112626.
- Xie, Y., Ren, J., Xu, J., 2022b. Underwater-art: Expanding information perspectives with text templates for underwater acoustic target recognition. *The Journal of the Acoustical Society of America* 152, 2641–2651.
- Xie, Y., Xiao, Y., Liu, X., Liu, G., Jiang, W., Qin, J., 2020. Time-frequency distribution map-based convolutional neural network (cnn) model for underwater pipeline leakage detection using acoustic signals. *Sensors*

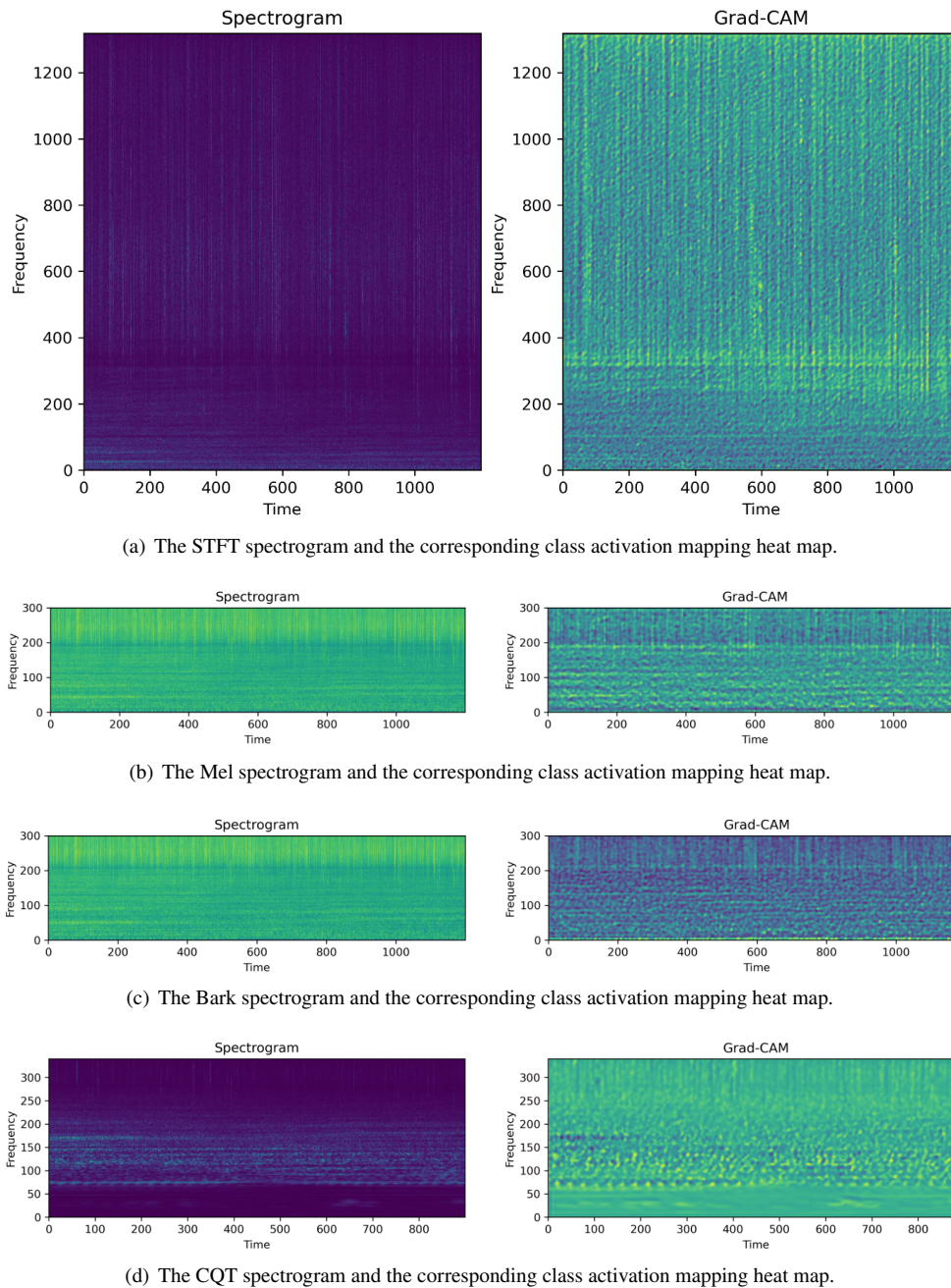


Figure 7: The spectrograms and their corresponding CAM heat maps across four features. We take the 30-second segment of a ro-ro ship in Shipsear as the example.

20, 5040.
 Yang, H., Gu, H., Yin, J., Yang, J., 2020. Gan-based sample expansion for underwater acoustic signal, in: Journal of Physics Conference Series, p. 012104.
 Yun, S., Han, D., Oh, S.J., Chun, S., Choe, J., Yoo, Y., 2019. Cutmix: Regularization strategy to train strong classifiers with localizable features, in: Proceedings of the IEEE/CVF international conference on computer vision, pp. 6023–6032.
 Zhang, H., Cisse, M., Dauphin, Y.N., Lopez-Paz, D., 2017. mixup: Beyond empirical risk minimization. arXiv preprint arXiv:1710.09412.
 Zhang, Q., Da, L., Zhang, Y., Hu, Y., 2021. Integrated neural networks based on feature fusion for underwater target recognition. Applied Acoustics 182, 108261.

Zhu, Y., Wang, B., Zhang, Y., Li, J., Wu, C., 2021. Convolutional neural network based filter bank multicarrier system for underwater acoustic communications. Applied Acoustics 177, 107920.